

Contents lists available at ScienceDirect

Ocean Engineering

journal homepage: www.elsevier.com/locate/oceaneng





Effect of zero-mean-shear turbulence on rise velocity of in-chain bubbles from marine natural seeps

Huijie Wu^a, Binbin Wang^{a,*}, Daniela Di Iorio^b, Mahdi Razaz^c

- a Department of Civil and Environmental Engineering, University of Missouri, Columbia, MO, 65211, United States
- ^b Department of Marine Sciences, University of Georgia, Athens, GA, 30602, United States
- c School of Ocean Science and Engineering, University of Southern Mississippi, Stennis Space Center, MS, 39529, United States

ARTICLE INFO

Keywords: Bubble Marine seep Ocean turbulence Oscillating grid-stirred turbulence

ABSTRACT

This paper reports on a laboratory experiment that investigates the impact of ocean turbulence on the rise velocity of bubbles released from natural seeps. To simulate the turbulence conditions of ocean bottoms, we used an oscillating grid-stirred turbulence (OGT) tank to generate nearly homogeneous and isotropic turbulence (HIT) with a range of turbulence dissipation rates. By isolating the effect of zero-mean-shear turbulence on the bubble rise from the effect of cross flows, we found that the presence of turbulence reduced the bubble rise velocity by up to 19% across six different gas flow rates. Our data show a linear relationship between the normalized bubble rise velocity and the log-value of the normalized turbulence dissipation rate, with two different slopes. Our analysis suggests that turbulence increased the horizontal motion of the bubbles, causing them to scatter laterally, thereby reducing their rise velocity. Lastly, we propose a semi-empirical equation that can be used to calculate the rise velocity of in-chain bubbles in turbulent waters. These findings have important implications for our understanding of the role of turbulence in the transport and fate of seep bubbles in ocean waters.

1. Introduction

Marine bubble seeps are an important carbon source for seafloor organisms and contribute to the vertical transport of hydrocarbons through bubbles rising in the water column (e.g., MacDonald et al., 2002; Römer et al., 2019; Wang et al., 2020; Razaz et al., 2020a). Bubbles form and emanate through various mechanisms from different types of sources, which determine their sizes, shapes, and group patterns of bubble rising (e.g., Leifer et al., 2009; Fu et al., 2021). When bubbles are released sequentially from a point source, they tend to form a chain-like structure, with the trailing bubbles rising in the wakes of the leading ones. This bubble-chain structure is notable for its ability to move through the water column with an enhanced mean rise velocity, a characteristic that has been demonstrated in laboratory experiments (Marks, 1973; Wang and Socolofsky, 2015b) and observed in the field (Razaz et al., 2020b). To achieve an increase in the rise velocity of bubbles, it is necessary for the bubbles to follow a nearly vertical path, i.e., forming a bubble chain. When cross flows are present but turbulence is low, they can disturb the structure of the bubble chain, leading to a reduction in the enhancement of the rise velocity of the bubbles (Wang and Socolofsky, 2015b). Nevertheless, turbulence is present ubiquitously near the ocean bottom, and there is no documented knowledge about how turbulence affects the rise velocity of in-chain bubbles. To fill this gap in understanding, we conducted an experimental study to examine the impact of turbulence, in the absence of mean shear, on the rise velocity of in-chain-bubbles.

When an isolated bubble rises in a liquid, the rising trajectory can vary among a straight line (one-dimensional), a zig-zag (twodimensional) curve, or a helical (three-dimensional) curve (Saffman, 1956; Clift et al., 1978; Wu and Gharib, 2002). Bubble size, shape, and the wake behind the rising bubble play an important role on the stability of the bubble path (de Vries et al., 2002; Wu and Gharib, 2002). These factors determine the force balance of the bubble rising through a liquid, and in turn govern its terminal rise velocity. Various bubble trajectories and their relationship with bubble rise velocities have been reported in natural bubble seeps using stereoscopic imaging systems (Wang and Socolofsky, 2015a; Wang et al., 2016). The different rising behaviors of bubbles are important indicators of bubble characteristics (e.g., surfactant-free vs. surfactant-coated), which is highly relevant to the dissolution of hydrocarbon in the water (Wang et al., 2016). The rise behavior of isolated bubbles has been the subject of extensive study, and a general consensus has been reached regarding the behavior of rising bubbles and the methods used to quantify their terminal velocity (e.g., Clift et al., 1978; Tomiyama et al., 1998, 2002;

E-mail address: wangbinb@missouri.edu (B. Wang).

^{*} Corresponding author.

Zheng and Yapa, 2000; Park et al., 2017). When bubbles are released in pairs that are adjacent to each other, the interactions between the two bubbles – such as potential effects, viscous corrections, and wake effects – can modify their paths of ascent, ultimately altering their rise velocities. (e.g., Wijngaarden, 1993; Yuan and Prosperetti, 1994; Brucker, 1999; Kusuno et al., 2019; Zhang and Ni, 2021).

When bubbles are continuously released from a single orifice or nozzle with relatively low flow rates, they rise in a chain-like structure. The wakes behind each bubble develop in a quasi-steady manner, resulting in a mean flow in the quiescent liquid and an enhanced bubble rise velocity (Marks, 1973; Ellingsen and Risso, 2001; Sanada et al., 2005; Wang and Socolofsky, 2015b, 2019). In this case, the drag coefficient can be modified to account for the effect of wake induced flow on the bubble rise velocity (Ruzicka, 2000). Recently, Liu et al. (2022) proposed a modified Weber number, incorporating a trigonometric relation, to better capture the dynamically varying drag coefficient experienced by bubbles rising within a chain. The mean water velocities induced by the in-chain-bubbles follow a near-Gaussian profile in the horizontal direction, resembling those found in pointsource jets and buoyancy-driven plumes (Wang and Socolofsky, 2019; Lee and Park, 2022). The turbulence characteristics of bubble-chain flows have been found to exhibit a non-strictly self-similar behavior due to the presence of two sets of scaling parameters within the gas-liquid two-phase system (Wang and Socolofsky, 2019). In bubble agitated flows, the dynamic length scale of the bubbly flow (Bombardelli et al., 2007; Wang et al., 2019) is important in characterizing both mean flow and turbulent parameters, including the characteristic length of wakes, turbulent kinetic energy and its dissipation rate (Wang and Socolofsky,

Several studies have attempted to investigate the effect of turbulence on the rise velocity of bubbles. Aliseda and Lasheras (2011) reported a reduction in the rise velocities of spherical bubbles (diameter D = 0.1–0.9 mm) under grid-generated turbulence with a horizontal mean flow ranging from 0.4-0.63 m/s. Poorte and Biesheuvel (2002) observed a decrease in the rise velocity of bubbles (D = 0.68 and 1.14 mm) of up to 35% under turbulence with a mean flow of 0.3 m/s, with turbulent fluctuating velocities ranging from 6%-44% of the bubble terminal velocity. Prakash et al. (2012) conducted an experiment in a vertical water tunnel with bubbles rising along with vertical mean flows of 0.2-0.6 m/s. They reported a reduction of approximately 20% in slip velocity of a 3-mm bubble with increasing turbulence of Kolmogorov length ranging 0.08–0.137D. Note that the 3-mm bubble used in their experiment is nearly spherical, with minimal deformation of the bubble-water interface due to the use of surfactant-treated water. Salibindla et al. (2020) investigated the effect of strong turbulence, characterized by a dissipation rate of turbulence kinetic energy ε = 0.5 m²/s³, on the rise velocity of bubbles in a vertical counterflow with jet-induced turbulence. The turbulence parameters used in the study were reported in Masuk et al. (2019). Salibindla et al. (2020) found that small bubbles (D < 2.2 mm) experienced suppressed rise velocities, while larger bubbles (D = 2.2-10 mm) exhibited enhanced rise velocities in the presence of turbulence.

The above studies provide valuable insights into the influence of turbulence on the rise behavior of bubbles. However, since these studies involved multiple bubbles and/or mean flow in the system, it is challenging to distinguish the effect of turbulence on the rise behavior of isolated bubbles from other factors. For example, changes in bubble rise velocity could be attributed to interactions between bubble-induced flow (e.g., bubble swarm or plume) and turbulence or mean water flow. To remove these factors, recently, Ruth et al. (2021) investigated the rise velocity of isolated bubbles with diameters ranging from 1 to 6 mm in intense turbulence generated using four submerged water pumps with $\epsilon = 0.002$ –0.319 m²/s³. They observed reductions in bubble rise velocity with increasing turbulence, and proposed a Froude number (Fr) scaling to quantify the turbulence effect on rise velocity of isolated bubbles. Fr was defined as $Fr = u'/\sqrt{gD}$ where u' represents the

characteristic turbulent fluctuation velocity and g is the gravitational acceleration. Table 1 summarizes the experimental conditions of all these studies. To provide the context of the turbulence effects on the maximal stable bubble diameter, the Hinze-scale is determined using $D_H(\rho/\sigma)^{3/5} \varepsilon^{2/5} = 0.725$, where ρ is the density of water, and σ is the interfacial tension between air and water (Hinze, 1955).

Our study aims to investigate the impact of turbulence on the mean rise velocity of in-chain bubbles. We hypothesize that turbulence would interfere with the bubble wakes, consequently affecting the rise behavior of bubbles. To differentiate the turbulence effect from cross-flow, we use homogeneous and isotropic turbulence (HIT), which eliminates any mean shear or horizontal/cross-flow velocities. A well studied zeromean-shear turbulence is the oscillating grid-stirred turbulence (OGT). In this study, we use a two-grid system OGT, which allows the in-chain bubbles to rise in zero-mean-shear turbulence with a series of wellcontrolled turbulence dissipation rates (Table 1). To simulate ocean bottom conditions, we selected a range of turbulence dissipation rates from 10^{-7} to $10^{-4}\ m^2/s^3$, as reported in the literature (Yang et al., 2021; Zulberti et al., 2022). As such, the objectives of this study are to verify whether the zero-mean-shear turbulence would affect the rise velocity of in-chain bubbles, and to develop a quantitative model for bubble rise velocity as a function of turbulence dissipation rate for bubble sizes commonly observed in natural seeps (Romer et al., 2012; Wang et al., 2016; Razaz et al., 2020b).

2. Methods

2.1. Bubble release in chains

The experiment was carried out in a rectangular tank with a dimension of $1\times0.35\times0.45$ m³ (Fig. 1). The water depth was maintained at 0.4 m, and the room temperature was approximately 22 °C. To release air bubbles in a chain-like structure, a 5 mm diameter orifice was placed at the center of the tank bottom. The experiment was conducted for six desired gas flow rates ($1 \le Q \le 90$ mL/min), which agree with the range of gas fluxes in natural seeps when bubbles are released in chain, Q < 100 mL/min (Wang et al., 2016). The size of the bubbles varied between 5 to 6 mm, and the spacing between neighboring bubbles ranged from 3 to 11 cm, except for the case of Q = 1 mL/min, where only one bubble was present in the water column. The bubbles were considered isolated in the case of Q = 1 mL/min.

To accurately control the bubble-release frequency and flow rate of the bubble chain, air flows were regulated using a syringe pump (NE-300 Just Infusion, New Era Pump Systems, Inc.) for flow rates $Q \leq 25$ mL/min. For Q > 25 mL/min, a mass flow controller (SmartTrak 100, Sierra Instruments) was used. Bubbles were released in both quiescent water and quasi-steady water with zero-mean-shear turbulence. A total of 10 different turbulence dissipation rates were used (Table 2, see Section 2.2 for details of turbulence).

2.2. Oscillating grid-stirred turbulence

In the region away from the grid and the wall boundaries of a OGT tank, the turbulent velocities generated by a single square bar grid can be quantified: $u' = C_1 Sf\left(x/M^{0.5}S^{0.5}\right)^{-\gamma}$ and $w' = C_2 u'$, where u' and w' are the root-mean-square (RMS) of the velocities parallel and perpendicular to the grid oscillating direction, respectively; x is the distance from the grid location; M is the mesh spacing; S is the stroke distance; and f is the oscillating frequency. The coefficients for the OGT model have been reported in the literature: γ ranges from 0.8 to 1.5, while C_1 and C_2 range from 0.2 to 0.5 and 1.1 to 1.4, respectively (Hopfinger and Linden, 1982; Brumley and Jirka, 1987; De Silva and Fernando, 1994). However, the OGT using a single grid naturally produces decaying turbulence and is often influenced by wall effects, leading to a large-scale mean flow in practical applications (e.g., McCorquodale and Munro, 2017). To mitigate turbulence decay and

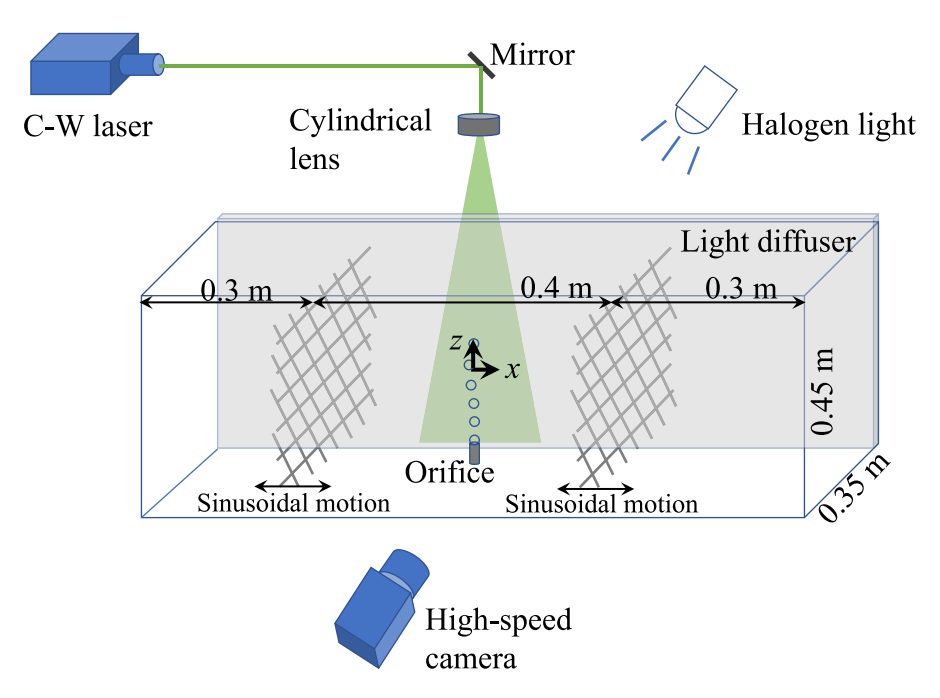


Fig. 1. Sketch of experimental setup.

Table 1 Summary of experimental studies in the literature about the effect of turbulence on bubble rise velocity. D: bubble diameter; \overline{U} : mean flow velocity; ε : turbulence dissipation rate; u': turbulence fluctuating velocity scale; η : Kolmogorov length; D_H : Hinze-scale.

Reference	D (mm)	\overline{U} (m/s)	ε (m ² /s ³)	u' (m/s)	η (mm)	D_H (mm)
Poorte and Biesheuvel (2002)	0.68 and 1.14	≈0.3	$9.5 \times 10^{-5} - 1 \times 10^{-2}$	0.016-0.058	0.10-0.32	15-96.3
Aliseda and Lasheras (2011)	0.1-0.9	0.4, 0.63	5×10^{-3} , 6×10^{-3}	0.1, 0.16	0.11, 0.12	18.3, 19.7
Prakash et al. (2012)	3	0.2-0.6	$3.5 \times 10^{-5} - 3 \times 10^{-4}$	Unknown	0.24-0.41	60.8-143.6
Salibindla et al. (2020)	0.5-10	Unknown	5×10^{-1}	0.25	0.038	3.1
Ruth et al. (2021)	1-6	≈0	$2 \times 10^{-3} - 3.2 \times 10^{-1}$	0.04-0.18	0.039-0.144	3.7-28.5
This study	5–6	0.0005-0.013	$3 \times 10^{-7} - 1.5 \times 10^{-4}$	0.003-0.027	0.29-1.35	80.2-963.6

minimize the mean flow, a two-grid system can be employed to generate a sufficiently large spatial scale of homogeneous and isotropic turbulence (HIT). Shy et al. (1997) demonstrated that a region of HIT up to 8 cm can be achieved using two oscillating grids.

In this study, OGT was driven by a pair of steel perforated sheets. The openings of the sheets are diamond-shaped, with diagonal lengths of 2 and 4.5 cm, which is equivalent to a 3-cm square mesh spacing with the same opening area. The sheets were mounted on the moving carriage of a heavy-load motorized linear stage (Zaber Technologies Inc.), which was programmed to travel back and forth with a sinusoidal wave form: $x = A \sin(2\pi t/T)$, where x is the travel distance, t is time, t is amplitude, and t is period of the wave form. Therefore, the stroke distance (t) and oscillating frequency (t) of the OGT were determined by t = 2t, t = 1/t.

In our experiment, we used three stroke distances (S = 1, 2, 4 cm) and three oscillating frequencies (f = 1, 2, 3 Hz), which gave nine combinations of turbulence conditions (Table 2). The grid Reynolds number $Re_G = MSf/v$ in our experiment spanned from 300 to 3600, where $v = 1 \times 10^{-6}$ m²/s is the kinematic viscosity of water. This configuration was optimized to ensure homogeneity and isotropy, with a grid solidity of less than 40%, an oscillation frequency below 7 Hz, and a stroke distance of less than 8 cm, as suggested in previous studies (McKenna and McGillis, 2004; McCorquodale and Munro, 2017).

2.3. Measurements

Two sets of measurements were carried out in this experiment sequentially. First, we applied particle image velocimetry (PIV) to measure the parameters of OGT. The flow field was seeded using

Table 2 Parameters of OGT in the experiment. S: stroke distance; f: oscillating frequency; Re_G : grid Revnolds number: ϵ : turbulence dissipation rate.

Case #	S (cm)	f (Hz)	Re_G (-)	ε (m ² /s ³)
Case 1	0	0	0	0
Case 2	1	1	300	0.3×10^{-6}
Case 3	1	2	600	2.4×10^{-6}
Case 4	1	3	900	6.8×10^{-6}
Case 5	2	1	600	1.3×10^{-6}
Case 6	2	2	1200	8.5×10^{-6}
Case 7	2	3	1800	3.3×10^{-5}
Case 8	4	1	1200	1.7×10^{-5}
Case 9	4	2	2400	5.7×10^{-5}
Case 10	4	3	3600	1.5×10^{-4}

polymaid particles with the median diameter of 15 μ m. A 532-nm 10-W continuous wave (C-W) laser (Laserglow Technologies) was used as the light source and a high-speed camera (Phantom VEO440L, Vision Research) was used for image acquisition. For each measurement run, 12 372 images with a dimension of 2560 \times 1600 pixel² were acquired continuously to the camera memory (72 GB) and then downloaded to a computer for later processing. Each run yielded 6186 velocity measurements within approximately 128.9 s. For each case, three runs were repeated to ensure the convergence of turbulence measurements.

Second, shadow-graphic imaging was used to measure bubble rise in the water. A halogen light was used as the light source and was diffused using a 3-mm thick translucent plate. Bubble images were recorded to the high-speed camera at 200 frames-per-second (fps). Three runs were repeated for each case, with each run taking 12 372 images, which correspond to approximately 185.6-s data. The physical resolution of

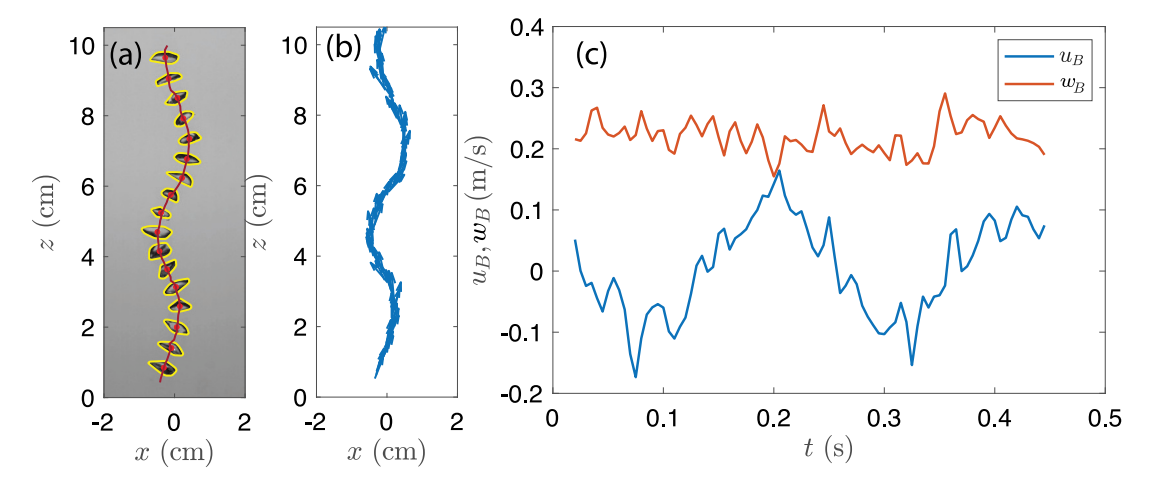


Fig. 2. (a) An example of bubble rising path (Note: isolated bubble rise in Case 4 turbulence; bubbles are shown every 5 time steps). The boundary and the center of each detected bubble are highlighted. The varying sizes observed in two-dimensional images are attributed to the effect of bubble deformation and the projection of different bubble orientations; (b) instantaneous velocity vectors along the bubble rising trajectory; (c) the time series of instantaneous bubble velocities in horizontal (u_B) and vertical (w_B) directions.

Table 3 Parameters of bubble rise experiment in quiescent (case 1) and turbulent water (case 2–10) for gas flow rate Q = 1 ml/min. D: bubble diameter; W_B : bubble rise velocity; Re_B : bubble Reynolds number; C_D : drag coefficient; We: Weber number.

Case	D (mm)	W_B (m/s)	Re _B (-)	C _D (-)	We (-)	
Q1-case1	5.1	0.237	1178	1.16	3.81	
Q1-case2	4.9	0.234	1152	1.18	3.68	
Q1-case3	5.0	0.230	1161	1.24	3.66	
Q1-case4	5.3	0.228	1205	1.34	3.75	
Q1-case5	5.0	0.227	1132	1.27	3.51	
Q1-case6	5.1	0.227	1153	1.29	3.58	
Q1-case7	5.2	0.231	1195	1.26	3.78	
Q1-case8	5.1	0.220	1114	1.36	3.35	
Q1-case9	5.1	0.240	1221	1.16	4.00	
Q1-case10	5.5	0.226	1217	1.44	3.70	

both PIV and shadow-graphic images was 6.54×10^{-5} m/pixel, giving the field of view (FOV) of 16.74×10.46 cm².

2.4. Data processing

PIV images were processed using an anti-aliased interrogation algorithm (Liao and Cowen, 2005) with a prediction–correction method at the final window of 24×24 pixel². With a physical resolution of 6.54×10^{-5} m/pixel, the window size of 24 pixels is equivalent to 1.6×10^{-3} m. Given that more than 95% of turbulence dissipation occurs at length scales $l > 2\pi\eta$, or wave numbers $k > \eta^{-1}$ where η is the Kolmogorov length scale (Cowen and Monismith, 1997), our PIV window size can resolve the turbulence dissipation when $\eta > 1.6 \times 10^{-3}/2\pi \approx 2.55 \times 10^{-4}$ m. This suggests that our PIV measurements adequately resolve dissipation rates $\varepsilon < v^3/\eta^4 = 2.6 \times 10^{-4}$ m²/s³. Therefore, all designed turbulence in this study satisfies this condition.

Mean flow and turbulence statistics were calculated from measured instantaneous velocities using Reynolds decomposition: u(t) = U + u'(t) and w(t) = W + w'(t). The turbulent velocity components u' and w' were used to determine the turbulence intensities $\sqrt{u'^2}$ and $\sqrt{w'^2}$, Reynolds shear stress $-\overline{u'w'}$, turbulence kinetic energy $k = 0.5(\overline{u'^2} + 2\overline{w'^2})$, and the rate of turbulence dissipation using a 'direct' method with an assumption of local isotropy (Luznik et al., 2007; Wang and Liao, 2016):

$$\varepsilon = 4\nu \left[\left(\frac{\partial u'}{\partial x} \right)^2 + \left(\frac{\partial w'}{\partial z} \right)^2 + \frac{3}{4} \left(\frac{\partial u'}{\partial z} \right)^2 + \frac{3}{4} \left(\frac{\partial w'}{\partial x} \right)^2 + \frac{3}{4} \left(\frac{\partial w'}{\partial x} \right)^2 \right]$$

$$+ \frac{\partial u'}{\partial x} \frac{\partial w'}{\partial z} + \frac{3}{2} \frac{\partial u'}{\partial z} \frac{\partial w'}{\partial z} \right]$$
(1)

Table 4 Parameters of bubble rise experiment in quiescent (case 1) and turbulent water (cases 2–10) for gas flow rate Q = 10.5 ml/min.

Case	D (mm)	W_B (m/s)	Re_B (-)	C_D (-)	We (-)
Q2-case1	5.2	0.257	1342	1.03	4.72
Q2-case2	5.2	0.257	1342	1.03	4.71
Q2-case3	5.2	0.256	1336	1.04	4.67
Q2-case4	5.1	0.252	1289	1.06	4.44
Q2-case5	5.2	0.255	1336	1.05	4.67
Q2-case6	5.4	0.243	1317	1.20	4.37
Q2-case7	5.1	0.249	1278	1.08	4.36
Q2-case8	5.2	0.239	1239	1.18	4.05
Q2-case9	5.5	0.240	1312	1.25	4.30
Q2-case10	5.2	0.220	1143	1.40	3.44

Shadow-graphic images were processed using an in-house MATLAB code for bubble detection and calculation of bubble rise velocity (Wang and Socolofsky, 2015b,a). We first converted images to gray-scale and applied a 'sobel' filter in the x-z plane of the images. A morphological structuring element of 4-pixel 'disk' was then used to dilate images to remove sharp edges and enhance foreground. Finally, a global threshold was used to convert images to the binary version with a 'hole-filling' function, resulting in a complete, individual bubble. The 'regionprops' function was used to determine the location (i.e., x and z coordinates) and size (i.e., occupied area and equivalent diameter) of each bubble. The equivalent spherical bubble diameter was determined using the projected area of the bubble as seen in the binary image. The data show the standard deviation of the determined bubble diameters in all images is within 20% of the mean bubble diameter. For instance, the mean diameter of Q1 cases is 5.1 mm, and the standard deviation of instantaneously determined bubble diameter is 0.7 mm, equivalently 14% of the mean diameter. The varying, instantaneously determined bubble diameters are attributed to the projection of bubbles with different orientations and bubble deformation (Fig. 2a).

Instantaneous bubble rise velocity was calculated from each pair of consecutive images using $w_B = \Delta z/\Delta t$ and the averaged bubble rise velocity (W_B) for all bubbles from all images was determined for each case. Similarly, the instantaneous horizontal bubble velocity can be obtained using $u_B = \Delta x/\Delta t$. The bubble rise trajectory is within the helical regime for the tested bubble sizes with correlated instantaneous bubble velocities (Fig. 2). The results of bubble rise velocity, bubble diameter, drag coefficient (C_D) , Weber number $(We = \rho W_B^2 D/\sigma)$ and bubble Reynolds number $(Re_B = W_B D/v)$ are summarized in Tables 3–8 for six different gas flow rates. The drag coefficient was determined from the equilibrium between the buoyancy and the drag force using $C_D = 4gD/(3W_B^2)$.

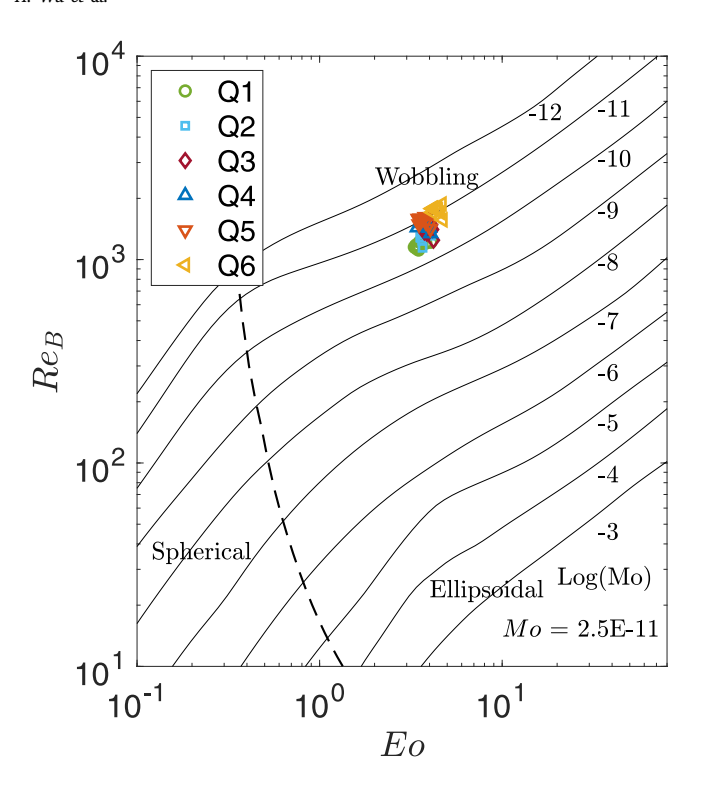


Fig. 3. Classification of shapes for the bubbles in this study. The $Eo-Re_B$ curves for each value of Mo are reproduced from Figure 2.5 in Clift et al. (1978).

The data show a typical deviation of approximately 10%–30% in the instantaneous bubble rise velocity from the mean bubble rise velocity, as measured over a 1/200-s time interval. The variation in velocity is due to the varying drag coefficient induced by vortex shedding in the bubble wake region (Liu et al., 2022). Additionally, the uncertainty of measurements may contribute to the observed velocity fluctuations. In particular, the uncertainty in the identified centroid of deformable bubbles in the two-dimensional images may introduce error in the measurement of instantaneous bubble rise velocity. This measurement uncertainty could become more pronounced with shorter time intervals. Because our study focuses on the mean bubble rise velocity averaged from multiple bubbles, we estimate that our estimation of bubble rise velocity has a measurement uncertainty of 10%, as determined by the standard deviation of all measured bubbles for each case.

The bubble shapes are examined based on the relationship among three dimensionless numbers: Eötvös number ($Eo = \Delta \rho g D^2/\sigma$), bubble Reynolds number (Re_B), and Morton number ($Mo = g \mu^4 \Delta \rho/\rho^2 \sigma^3$), where μ is dynamic viscosity of water and $\Delta \rho$ is the difference in densities between water and air bubbles (Clift et al., 1978). The analysis of shadow-imaging data reveals that all bubbles fall within the ellipsoidal and wobbling regime (Fig. 3). We did not observe significant changes in shapes for the turbulence conditions tested in this study (See supplementary videos).

3. Results and discussion

3.1. Oscillating grid-stirred turbulence

The PIV measurements confirm that the flow exhibited zero-mean velocity, and that the turbulence was nearly isotropic. The data indicates a nearly-Gaussian velocity distribution, with mean values close to zero in both the x and z directions, and the ratio between turbulence intensities $\sqrt{u'^2}/\sqrt{w'^2}=1.17$ (Fig. 4). This value falls within the reported range of OGT using a single grid, i.e., 1.1–1.4 (Hopfinger

Table 5 Parameters of bubble rise experiment in quiescent (case 1) and turbulent water (cases 2–10) for gas flow rate Q = 25.0 ml/min.

Case	D (mm)	W_B (m/s)	Re_B (-)	C_D (-)	We (-)
Q3-case1	5.4	0.270	1481	0.99	5.46
Q3-case2	5.4	0.272	1453	0.95	5.39
Q3-case3	5.3	0.269	1438	0.96	5.30
Q3-case4	5.3	0.269	1423	0.96	5.23
Q3-case5	5.4	0.264	1427	1.01	5.16
Q3-case6	5.3	0.263	1386	1.00	4.98
Q3-case7	5.3	0.254	1353	1.08	4.70
Q3-case8	5.2	0.261	1368	1.01	4.87
Q3-case9	5.2	0.254	1406	1.12	4.89
Q3-case10	5.6	0.224	1246	1.45	3.82

Table 6 Parameters of bubble rise experiment in quiescent (case 1) and turbulent water (cases 2–10) for gas flow rate Q = 50.0 ml/min.

Case	D (mm)	W_B (m/s)	Re_B (-)	C_D (-)	We (-)
Q4-case1	5.3	0.292	1535	0.81	6.12
Q4-case2	5.2	0.292	1531	0.80	6.12
Q4-case3	5.2	0.296	1525	0.77	6.17
Q4-case4	5.3	0.293	1541	0.80	6.17
Q4-case5	5.2	0.296	1538	0.78	6.22
Q4-case6	5.2	0.291	1506	0.80	5.99
Q4-case7	5.3	0.285	1511	0.86	5.88
Q4-case8	5.0	0.286	1436	0.80	5.62
Q4-case9	5.4	0.264	1429	1.02	5.15
Q4-case10	5.5	0.246	1343	1.18	4.52

Table 7 Parameters of bubble rise experiment in quiescent (case 1) and turbulent water (cases 2–10) for gas flow rate Q = 70.0 ml/min.

Case	D (mm)	W_B (m/s)	Re_B (-)	C_D (-)	W e (-)
Q5-case1	5.2	0.315	1590	0.67	6.85
Q5-case2	5.1	0.312	1596	0.69	6.81
Q5-case3	5.1	0.309	1578	0.70	6.67
Q5-case4	5.3	0.308	1623	0.73	6.84
Q5-case5	5.1	0.311	1574	0.69	6.69
Q5-case6	5.2	0.305	1574	0.72	6.57
Q5-case7	5.3	0.290	1523	0.83	6.07
Q5-case8	5.1	0.295	1494	0.77	6.02
Q5-case9	5.4	0.278	1507	0.92	5.72
Q5-case10	5.5	0.261	1421	1.05	5.06

Table 8 Parameters of bubble rise experiment in quiescent (case 1) and turbulent water (cases 2–10) for gas flow rate Q = 90.0 ml/min.

Case	D (mm)	W_B (m/s)	Re_B (-)	C_D (-)	We (-)
Q6-case1	5.5	0.323	1780	0.69	7.86
Q6-case2	5.6	0.323	1792	0.70	7.90
Q6-case3	5.5	0.321	1778	0.71	7.80
Q6-case4	5.9	0.320	1877	0.75	8.22
Q6-case5	5.6	0.320	1774	0.71	7.75
Q6-case6	5.7	0.315	1796	0.75	7.74
Q6-case7	5.7	0.305	1749	0.80	7.30
Q6-case8	5.5	0.309	1708	0.75	7.22
Q6-case9	5.8	0.293	1703	0.88	6.83
Q6-case10	5.9	0.266	1567	1.09	5.69

and Linden, 1982; Brumley and Jirka, 1987; De Silva and Fernando, 1994), and the range of OGT generated by a pair of grids, i.e., 1.05-1.30 (Shy et al., 1997; Hoque et al., 2015). For all 9 cases, the median value of ratios between the root-mean-square (RMS) of the velocity fluctuations and the mean velocity is 2.1. This is better than the paired-grid OGT tank in Shy et al. (1997), where the ratios are close to 1. Shy et al. (1997) reported that, within a 20 cm distance between the two grids, the middle 8-cm region exhibited near-homogeneous turbulence. The near-homogeneous region of turbulence increases with the distance between the grid pair. Our tank also exhibited an approximately 8-cm homogeneous region in the x direction, resulting in a ratio between the

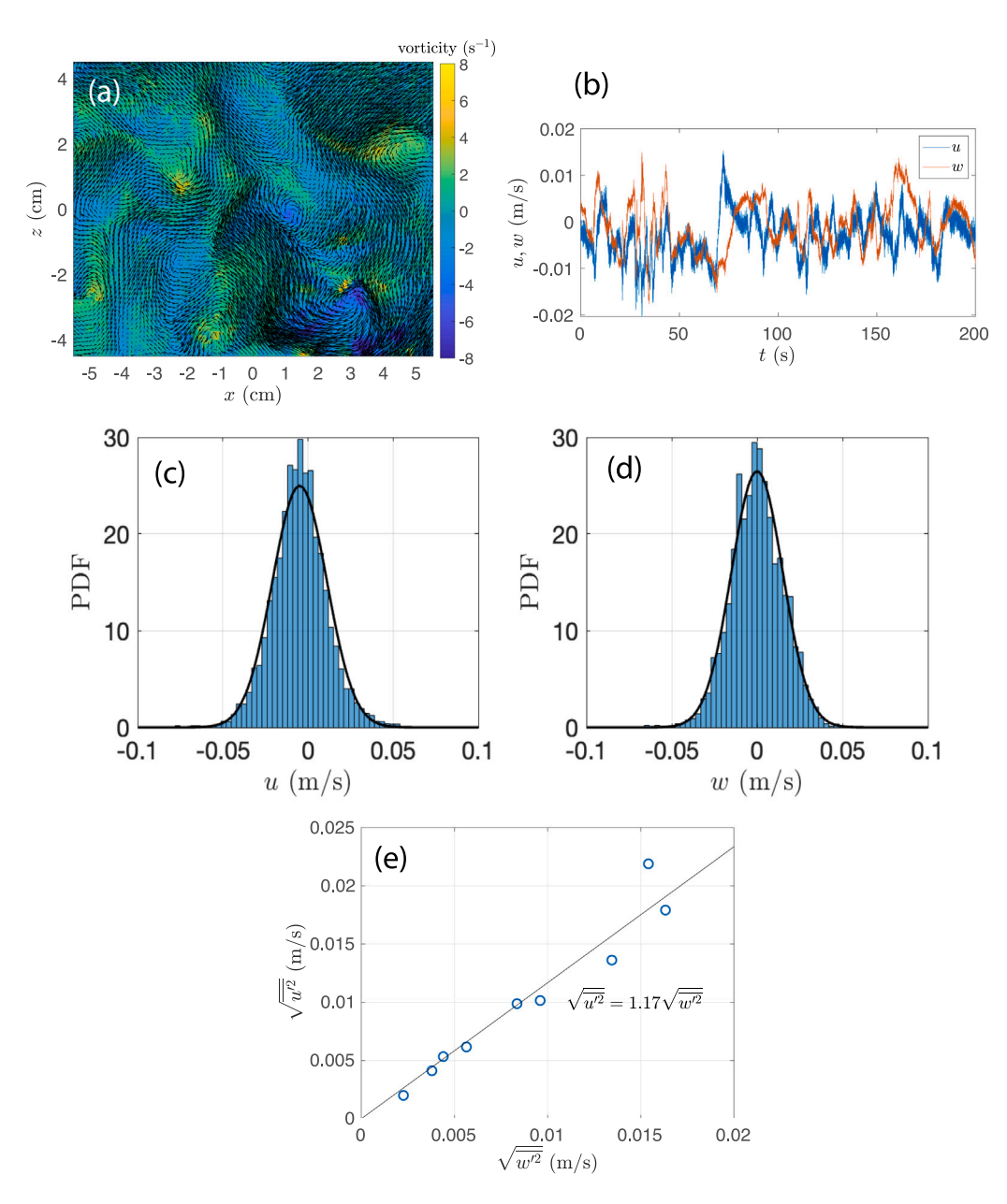


Fig. 4. (a) An example of flow field in the oscillating grid-stirred turbulence (OGT) tank measured using PIV (Case 4: S = 1 cm, f = 3 Hz). Velocity vectors are plotted with superposition of vorticity; (b) a 200-s time series of instantaneous velocity at the center of the PIV field of view (FOV); (c-d) probability density function (PDF) of the instantaneous velocities. The solid black lines show the Gaussian fit to the velocity distributions; (e) the ratio of turbulence intensities for 9 OGT cases.

standard deviation and mean of ε less than 10%. This ratio increases to 30% within a 12-cm region due to the asymmetric effect of grid oscillation, which is stronger near the edges of the region.

For $\varepsilon=10^{-7}\sim 10^{-4}~\text{m}^2/\text{s}^3$, the data reveal that ε increases with increasing S under constant f, and with increasing f under constant S (Fig. 5). The increase in ε is caused by stronger wake turbulence generated at the grid location, which can result from either longer stokes or higher stir frequencies. The monotonically increase of ε with f under constant S was also found in much stronger OGT ($\varepsilon=10^{-3}\sim 10^{-1}~\text{m}^2/\text{s}^3$) generated by a pair of grids (Hoque et al., 2015). A power law relationship between ε and grid Reynolds number was determined in the region of nearly homogeneous and isotropic turbulence by fitting the data using a non-linear least squares regression. The resulting equation is $\varepsilon=2.2\times 10^{-13}~\text{Re}_G^{2.5}$ (Fig. 6). This equation unifies the two parameters responsible for the increase in turbulence.

3.2. In-chain-bubble rise in quiescent water

The results presented in Fig. 7 illustrate the increase in the rise velocity (W_B) of in-chain bubbles with increasing gas flow rate (Q). The observed trend is in agreement with previously reported data (Marks, 1973; Wang and Socolofsky, 2015b). The small discrepancy between our data and those literature data is likely due to the difference in water properties that contribute to the density, surface tension, and viscosity, which affect the rise velocity of the bubbles. A non-dimensional format of bubble rise velocity as a function of gas flow rate can be derived using the theory of wake flows behind a sphere (Marks, 1973; Wang and Socolofsky, 2015b), giving:

$$\left(\frac{W_B}{W_0}\right)^{5/3} - \left(\frac{W_B}{W_0}\right)^{2/3} \propto \left(\frac{12gQ^2}{\pi\beta^2 W_0^4 D^3}\right)^{1/3} \tag{2}$$

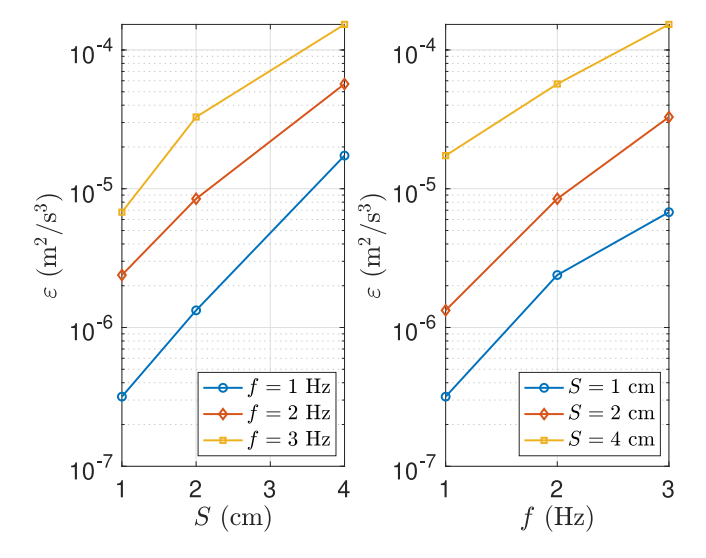


Fig. 5. Measured turbulence dissipation rate as a function of grid stroke distance S and oscillating frequency f.

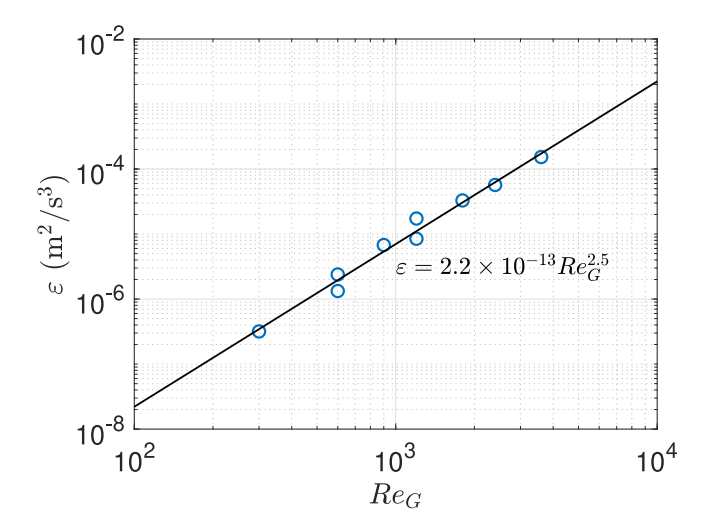


Fig. 6. Measured turbulence dissipation rate as a function of grid Reynolds number.

where W_0 is the terminal velocity of isolated bubbles with the same diameter, g is gravitational acceleration, and β is a coefficient related to the ratio between the mixing length and the half-width of the wake (Schlichting, 1979).

Fig. 7b presents a non-dimensional format of the relationship between bubble rise velocity and gas flow rate. The results of the linear regression show $\left(W_B/W_0\right)^{5/3}-\left(W_B/W_0\right)^{2/3}=1.5\left(gQ^2/(W_0^4D^3)\right)^{1/3}-0.05$, indicating that the enhancement of bubble rise velocity is primarily due to the superposition of wake flow onto the terminal velocity of isolated bubbles. This relationship has been directly validated in Wang and Socolofsky (2019).

3.3. In-chain-bubble rise in zero-mean-shear turbulent water

The effect of zero-mean-shear turbulence on bubble rise is illustrated in Fig. 8. For S=1 cm, the data show that bubble rise velocity decreases as f increases, including the isolated bubble. Our result seems to support that the terminal velocity of an isolated bubble may be reduced by turbulence. This result agrees with the study in Ruth et al. (2021), who reported that the reduction in bubble rise velocity is a function of turbulence-based Froude number. In our experiments, the bubbles had Froude numbers ranging from 0.12 to 0.36, which

correspond to a weak velocity reduction region (reduction < 10%) in the analysis of Fr-scaling (Ruth et al., 2021). We observed up to a 6.8% reduction in bubble rise velocity within this Fr range. We note that, in the weak velocity reduction region, there is noticeable scattering in the available literature data (Poorte and Biesheuvel, 2002; Prakash et al., 2012; Ruth et al., 2021).

In bubble-chain cases, the reduction of bubble rise velocity with increasing f becomes more substantial as S increases. As an example, at the highest flow rate (Q6), for S=4 cm, the bubble rise velocity decreased from 0.31 to 0.27 m/s as f increased from 1 to 3 Hz. This corresponds to reductions of 4.3% and 17.7% from the bubble rise velocity of 0.32 m/s in quiescent water.

The quantitative relationship between W_B and ε is given in Fig. 9, elucidating decreasing W_B with increasing ε . In quiescent water, the bubble-chain effect is reflected in the enhanced W_B from 0.23 to 0.32 m/s from Q1 to Q6. For $\varepsilon=1.5\times 10^{-4}$ m²/s³, the bubble-chain effect was reduced, resulting in a range of W_B values from 0.22 to 0.27 m/s. Mechanistically, the effect of bubble-chain is that wake-induced flows of leading bubbles are superimposed onto the terminal velocity of isolated bubbles (Wang and Socolofsky, 2015b). Thus, the reduction of bubble-chain effect must be caused by the turbulence effect on the wake flow of leading bubbles. Notably, the bubble-chain effect on bubble rise velocity was found to be completely absent in Cases Q1 to Q3 when subjected to the strongest turbulence (Case 10). This observation suggests that the turbulence effect completely diminishes the bubble-chain effect on the bubble rise velocity in these cases.

To model the turbulence-induced suppression of wake-enhanced bubble rise velocity, we analyzed the bubble rise velocity and turbulence dissipation rate in a normalized format (Fig. 10). Here, bubble rise velocity (W_B) is normalized with that in quiescent water (W_{B0}), and turbulence dissipation rate is normalized with a value representing a turbulent flow is too weak to disrupt bubble wakes (ε_0). We define this critical value in the turbulence where the Kolmogorov length scale (η) is equal to the bubble diameter. For the bubble diameter of 5–6 mm used in this experiment, this critical dissipation rate was calculated to be on the order of $\varepsilon_0 = v^3/\eta^4 \sim 10^{-9} \text{ m}^2/\text{s}^3$. Therefore, the percentage of rise velocity compared to its value in quiescent water (W_B/W_{B0}) due to turbulence suppression is determined by the order of magnitude difference in the dissipation rate compared with the critical dissipation rate ($\log_{10}(\varepsilon/\varepsilon_0)$). We obtained a regression equation that models this relationship:

$$\frac{W_B}{W_{B0}} = \begin{cases}
1.0 - 0.013 \log_{10}(\epsilon/\epsilon_0) & \text{for } \log_{10}(\epsilon/\epsilon_0) < 4 \\
\min\left(1.5 - 0.125 \log_{10}(\epsilon/\epsilon_0), \frac{W_0}{W_{B0}}\right) & \text{for } \log_{10}(\epsilon/\epsilon_0) > 4
\end{cases}$$
(3)

Recall that the normalized W_{B0} using the isolated bubble rise velocity (W_0) can be parameterized using a non-dimensional format of gas flow rate $(gQ^2/W_0^4D^3)$ (Wang and Socolofsky, 2015b). Our data show:

$$\frac{W_{B0}}{W_0} = 1 + 1.07 \left(\frac{gQ^2}{W_0^4 D^3}\right)^{1/3} \tag{4}$$

The in-chain bubble rise velocity in zero-mean-shear turbulent water can be calculated as a function of bubble diameter, gas flow rate, and turbulence dissipation rate by combining Eqs. (3) and (4). The resulting calculated bubble rise velocities are plotted against the measured data in Fig. 11. The comparison shows a good agreement between the measured data and the predicted results using the empirical equation, with a high R-squared value of 0.97 and a low root-mean-square-error (RMSE) of 0.0052 m/s. It is important to note that the validity of the equation is limited to the measured data range, which corresponds to continuously released bubbles from a single orifice without bubble breakup, and where the turbulence dissipation rate is less than 2×10^{-4} m²/s³ and the gas flow rate is less than 100 mL/min.

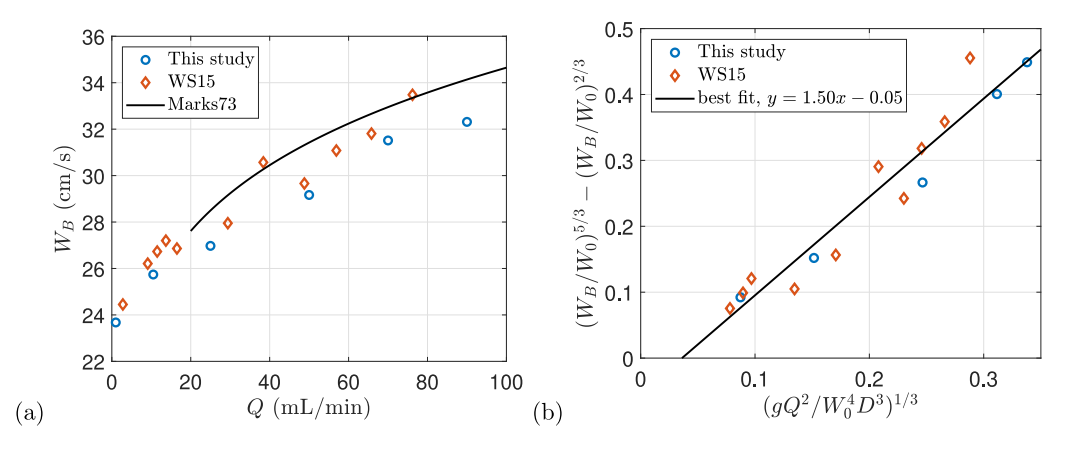


Fig. 7. Bubble rise velocity as a function of gas flow rate: (a) in physical scale; (b) in normalized scale. Normalization is derived using bubble wake theory. 'WS15' shows the data collected in Wang and Socolofsky (2015b). 'Marks73' shows the best-fit relation of data collected in Marks (1973): $W_B = 18.1Q^{0.141}$ for Q > 20 mL/min, where the unit of W_B and Q takes cm/s and mL/min, respectively.

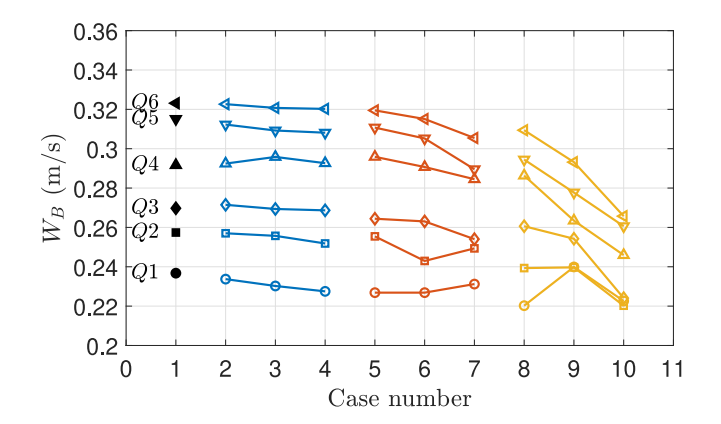
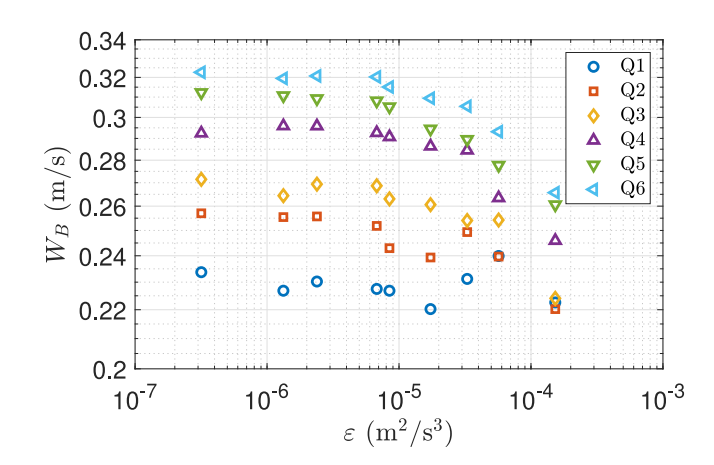


Fig. 8. Bubble rise velocity in different cases shows the influence of grid oscillating frequency (f) and stroke distance (S) on rise velocity of in-chain bubbles. Case 1 (closed symbols): quiescent water; Cases 2-4: S=1 cm, f=1-3 Hz, Cases 5-7: S=2 cm, f=1-3 Hz, Cases 8-10: S=4 cm, f=1-3 Hz. Different symbols indicate different gas flow rates.



 $\textbf{Fig. 9.} \ \, \textbf{Bubble} \ \, \textbf{rise} \ \, \textbf{velocity} \ \, \textbf{as} \ \, \textbf{a} \ \, \textbf{function} \ \, \textbf{of turbulence} \ \, \textbf{dissipation} \ \, \textbf{rate} \ \, \textbf{at} \ \, \textbf{different} \ \, \textbf{gas} \ \, \textbf{flow} \ \, \textbf{rates}.$

3.4. Behavior of in-chain bubbles in turbulent water

To gain insights into the mechanisms underlying the reduction in bubble rise velocity due to turbulence, we analyzed the differences in bubble rise trajectories between quiescent and turbulent waters (Fig. 12). For instance, at a flow rate of 90 mL/min in quiescent

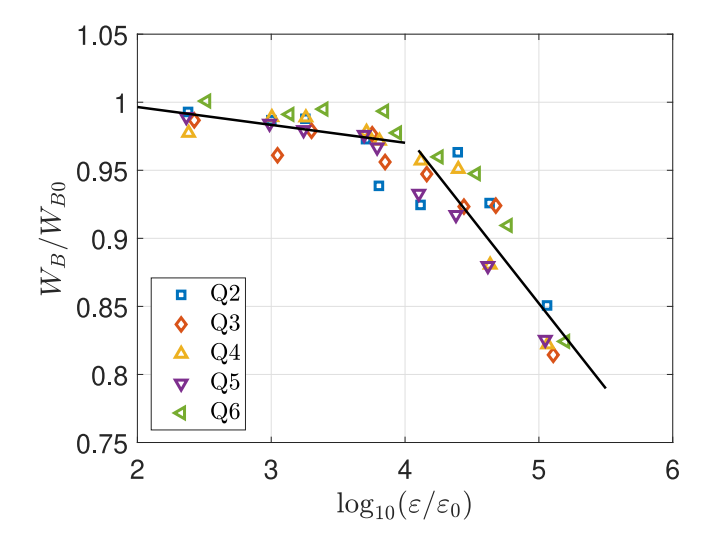


Fig. 10. Normalized bubble rise velocity as a function of normalized turbulence dissipation rate. Two solid lines show the best fit relationships to describe the effect of dissipation rate on the bubble rise velocity. The fitted equations are given in Eq. (3).

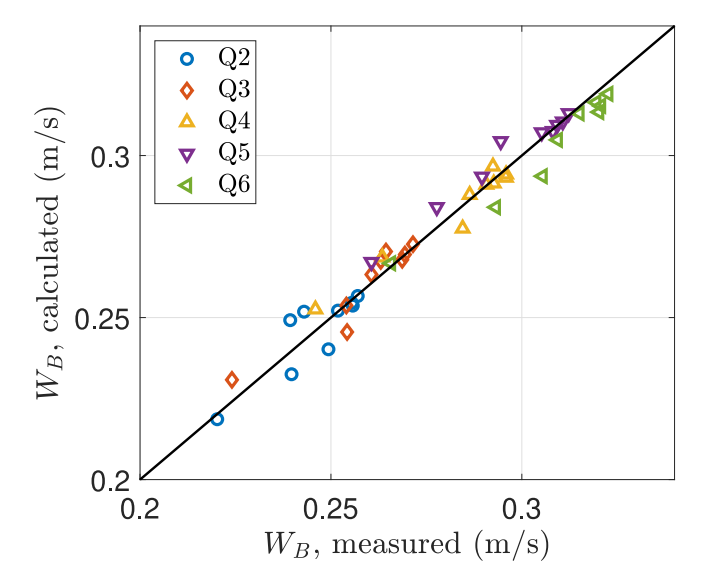


Fig. 11. Comparison between measured and modeled bubble rise velocities for bubble-chain flows under turbulence without mean shear.

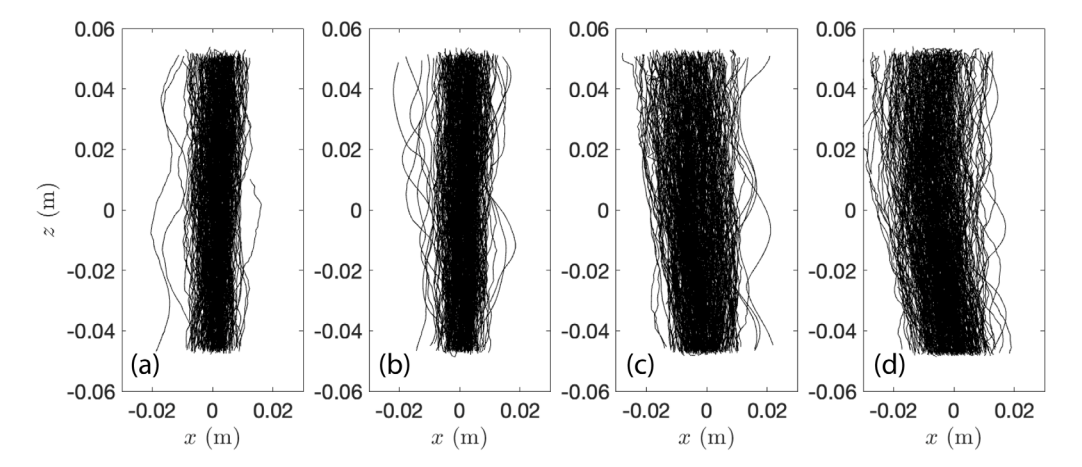


Fig. 12. Trajectories of in-chain bubbles (Q6: 90 mL/min) in quiescent and turbulent waters with different turbulence dissipation rates: (a) quiescent water; (b) Case 4 ($\varepsilon = 6.8 \times 10^{-6}$ m²/s³); (c) Case 7 ($\varepsilon = 3.3 \times 10^{-5}$ m²/s³); (d) Case 10 ($\varepsilon = 1.5 \times 10^{-4}$ m²/s³).

waters, bubbles mostly rose within a horizontal width of less than 2 cm. The superposition of bubble wakes within this narrow region resulted in an enhanced bubble rise velocity (Wang and Socolofsky, 2015b). However, as turbulence increased, the width of the rising paths also increased, reaching up to twice the width in quiescent water when the turbulence dissipation rate was $1.5 \times 10^{-4}~\text{m}^2/\text{s}^3$. While the number of bubble wakes remained constant, they spread out over a wider rising region, thus reducing the effect of wake superposition and leading to a reduction in bubble rise velocity.

Additionally, we observed a slight increase in the mean horizontal velocity magnitude with increasing turbulence, from 5.2 to 5.8 cm/s, at $\varepsilon=1.5\times10^{-4}~\text{m}^2/\text{s}^3$. Our data also revealed that the instantaneous horizontal velocity weakly but negatively correlated with the instantaneous rise velocity (also reported by Lee and Park, 2022). Taken together, our observations suggest that turbulence enhances the horizontal movement of bubbles, including lateral velocity and travel distance, which in turn contributes to the reduction of the wake effect on bubble rise and ultimately leads to a reduction in bubble rise velocity.

Our observations suggest that the reduction in bubble rise velocity is primarily due to the reduction in the superposition of bubble wakes onto the terminal velocity of isolated bubbles. This mechanism is similar to but distinct from the effects observed in cross-flow conditions, in which the bubbles are advected by the cross-flow and displaced from the center of the wake in the same direction (Wang and Socolofsky, 2015b). In contrast, turbulence can induce a variety of bubble motions in different directions, and may also alter the characteristics of the bubble wake. Therefore, to fully understand the interactions between turbulence and bubbles, it will be necessary to simultaneously measure both the bubble and turbulence fields, which is subject to future studies.

4. Conclusions

In this laboratory experiment, we aimed to investigate the impact of ocean turbulence on the rise velocity of bubbles released from natural seeps. We began by validating the homogeneous and isotropic turbulence (HIT) in the desired region of the oscillating grid-stirred turbulence (OGT) tank using a pair of steel perforated sheets. Next, we released a series of seep-like bubble streams into the HIT region, allowing us to evaluate the effect of zero-mean-shear turbulence on the rise velocity of in-chain bubbles.

Our analysis reveals that the instantaneous velocities in both horizontal and vertical directions in the OGT follow a near-Gaussian distribution. The ratio between turbulence intensities is approximately 1.17, indicating that the turbulence is isotropic. The HIT region of the OGT is 8 cm, within which the standard deviation of turbulence

dissipation rate is less than 10% of the mean value. We also observed that the turbulence dissipation rate scales with the grid Reynolds number according to a power-law relation.

In quiescent water, in-chain bubbles rise with an increased mean velocity due to the superposition of wake-induced water velocity on the slip velocity of bubbles. However, zero-mean-shear turbulence effectively disrupts this enhancement, resulting in a reduction of the bubble rise velocity. Our data analysis shows that, in the ocean bottom turbulence ($\varepsilon = 10^{-7}$ to 10^{-4} m²/s³), the normalized bubble rise velocity has a linear relationship with the log-values of normalized turbulence dissipation rate, with two different slopes: W_B/W_{B0} ~ $-0.013 \log_{10}(\varepsilon/\varepsilon_0)$ for $\log_{10}(\varepsilon/\varepsilon_0) < 4$, and $W_B/W_{B0} \sim -0.125 \log_{10}(\varepsilon/\varepsilon_0)$ for $\log_{10}(\epsilon/\epsilon_0) > 4$. Using the wake theory and the empirical equation obtained through regression, we developed an equation to determine in-chain bubble rise velocity in zero-mean-shear turbulent water. Our analysis suggests that the reduction of bubble rise velocity is likely due to the turbulence-induced enhancement of bubble lateral motions that reduce the superposition of wake-induced water flow onto the bubble slip velocities.

CRediT authorship contribution statement

Huijie Wu: Methodology, Formal analysis, Investigation, Data curation, Writing – original draft. **Binbin Wang:** Conceptualization, Methodology, Resources, Data curation, Investigation, Validation, Resources, Writing – original draft, Supervision, Project administration, Funding acquisition. **Daniela Di Iorio:** Conceptualization, Writing – original draft, Writing – review & editing. **Mahdi Razaz:** Conceptualization, Writing – original draft, Writing – review & editing.

Declaration of competing interest

The authors declare that they have no known competing financial interests or personal relationships that could have appeared to influence the work reported in this paper.

Data availability

Data will be made available on request.

Acknowledgments

The authors are grateful for the support from the National Science Foundation, United States (Award number 2049415).

Appendix A. Supplementary data

Supplementary material related to this article can be found online at https://doi.org/10.1016/j.oceaneng.2023.114810.

References

- Aliseda, A., Lasheras, J.C., 2011. Preferential concentration and rise velocity reduction of bubbles immersed in a homogeneous and isotropic turbulent flow. Phys. Fluids 23 (9), 093301. http://dx.doi.org/10.1063/1.3626404.
- Bombardelli, F.A., Buscaglia, G.C., Rehmann, C.R., Rincon, L.E., Garcia, M.H., 2007.
 Modeling and scaling of aeration bubble plumes: A two-phase flow analysis. J.
 Hydraul. Res. 45, 617–630. http://dx.doi.org/10.1080/00221686.2007.9521798.
- Brucker, C., 1999. Structure and dynamics of the wake of bubbles and its relevance bubble interaction. Phys. Fluids 11, 1781–1796. http://dx.doi.org/10.1063/
- Brumley, B.H., Jirka, G.H., 1987. Near-surface turbulence in a grid-stirred tank. J. Fluid Mech. 183, 235–263. http://dx.doi.org/10.1017/S0022112087002623.
- Clift, R., Grace, J.R., Weber, M.E., 1978. Bubbles, Drops, and Particles. Academic Press.
 Cowen, E., Monismith, S., 1997. A hybrid digital particle tracking velocimetry technique. Exp. Fluids 22, 199–211. http://dx.doi.org/10.1007/s003480050038.
- De Silva, I.P.D., Fernando, H.J.S., 1994. Oscillating grids as a source of nearly isotropic turbulence. Phys. Fluids 6 (7), 2455–2464. http://dx.doi.org/10.1063/1.868193.
- de Vries, A., Biesheuvel, A., van Wijngaarden, L., 2002. Notes on the path and wake of a gas bubble rising in pure water. Int. J. Multiph. Flow. (ISSN: 0301-9322) 28 (11), 1823–1835. http://dx.doi.org/10.1016/S0301-9322(02)00036-8.
- Ellingsen, K., Risso, F., 2001. On the rise of an ellipsoidal bubble in water: oscillatory paths and liquid-liquid velocity. J. Fluid Mech. 440, 235–268. http://dx.doi.org/10.1017/S0022112001004761.
- Fu, X., Waite, W.F., Ruppel, C.D., 2021. Hydrate formation on marine seep bubbles and the implications for water column methane dissolution. J. Geophys. Res.: Oceans 126 (9), e2021JC017363. http://dx.doi.org/10.1029/2021JC017363.
- Hinze, J.O., 1955. Fundamentals of the hydrodynamic mechanism of splitting in dispersion processes. AIChE J. 1 (3), 289–295. http://dx.doi.org/10.1002/aic. 690010303.
- Hopfinger, E.J., Linden, P.F., 1982. Formation of thermoclines in zero-mean-shear turbulence subjected to a stabilizing buoyancy flux. J. Fluid Mech. 114, 157–173. http://dx.doi.org/10.1017/S0022112082000081.
- Hoque, M.M., Sathe, M.J., Mitra, S., Joshi, J.B., Evans, G.M., 2015. Comparison of specific energy dissipation rate calculation methodologies utilising 2D PIV velocity measurement. Chem. Eng. Sci. (ISSN: 0009-2509) 137, 752–767. http://dx.doi.org/ 10.1016/j.ces.2015.06.056.
- Kusuno, H., Yamamoto, H., Sanada, T., 2019. Lift force acting on a pair of clean bubbles rising in-line. Phys. Fluids 31 (7), 072105. http://dx.doi.org/10.1063/1.5100183.
- Lee, J., Park, H., 2022. Flow induced by the single-bubble chain depending on the bubble release frequency. Phys. Fluids 34 (3), 033312. http://dx.doi.org/10.1063/ 5.0083281.
- Leifer, I., Jeuthe, H., Gjøsund, S.H., Johansen, V., 2009. Engineered and natural marine seep, bubble-driven buoyancy flows. J. Phys. Oceanogr. 39 (12), 3071–3090. http://dx.doi.org/10.1175/2009JPO4135.1.
- Liao, Q., Cowen, E.A., 2005. An efficient anti-aliasing spectral continuous window shifting technique for PIV. Exp. Fluids 38 (2), 197–208. http://dx.doi.org/10.1007/ s00348-004-0899-7.
- Liu, M., Wang, b., Tan, L., 2022. Correlation of drag coefficient between rising bubbles in chain. Phys. Fluids 34 (4), 043314. http://dx.doi.org/10.1063/5.0088375.
- Luznik, L., Gurka, R., Nimmo Smith, W.A.M., Zhu, W., Katz, J., Osborn, T.R., 2007.
 Distribution of energy spectra, Reynolds stresses, turbulence production, and dissipation in a tidally driven bottom boundary layer. J. Phys. Oceanogr. 37 (6), 1527–1550. http://dx.doi.org/10.1175/Jpo3076.1.
- MacDonald, I.R., Leifer, I., Sassen, R., Stine, P., Mitchell, R., Guinasso, Jr., N., 2002. Transfer of hydrocarbons from natural seeps to the water column and atmosphere. Geofluids 2 (2), 95–107. http://dx.doi.org/10.1046/j.1468-8123.2002.00023.x.
- Marks, C.H., 1973. Measurements of the terminal velocity of bubbles rising in chain. ASME J. Fluid Eng. 95, 17–22.
- Masuk, A.U.M., Salibindla, A., Tan, S., Ni, R., 2019. V-ONSET (vertical octagonal noncorrosive stirred energetic turbulence): A vertical water tunnel with a large energy dissipation rate to study bubble/droplet deformation and breakup in strong turbulence. Rev. Sci. Instrum. 90 (8), 085105. http://dx.doi.org/10.1063/1.5093688.
- McCorquodale, M.W., Munro, R.J., 2017. Experimental study of oscillating-grid turbulence interacting with a solid boundary. J. Fluid Mech. 813, 768–798. http://dx.doi.org/10.1017/jfm.2016.843.
- McKenna, S.P., McGillis, W.R., 2004. Observations of flow repeatability and secondary circulation in an oscillating grid-stirred tank. Phys. Fluids 16 (9), 3499–3502. http://dx.doi.org/10.1063/1.1779671.

- Park, S.H., Park, C., Lee, J., Lee, B., 2017. A simple parameterization for the rising velocity of bubbles in a liquid pool. Nucl. Eng. Technol. (ISSN: 1738-5733) 49 (4), 692-699. http://dx.doi.org/10.1016/j.net.2016.12.006.
- Poorte, R.E.G., Biesheuvel, A., 2002. Experiments on the motion of gas bubbles in turbulence generated by an active grid. J. Fluid Mech. 461, 127–154. http://dx. doi.org/10.1017/S0022112002008273.
- Prakash, V.N., Tagawa, Y., Calzavarini, E., Mercado, J.M., Toschi, F., Lohse, D., Sun, C., 2012. How gravity and size affect the acceleration statistics of bubbles in turbulence. New J. Phys. 14 (10), 105017. http://dx.doi.org/10.1088/1367-2630/14/10/105017.
- Razaz, M., Di Iorio, D., Wang, B., Asl, S.D., Thurnherr, A.M., 2020a. Variability of a natural hydrocarbon seep and its connection to the ocean surface. Sci. Rep. 10, 12654. http://dx.doi.org/10.1038/s41598-020-68807-4.
- Razaz, M., Iorio, D.D., Wang, B., MacDonald, I., 2020b. Temporal variations of a natural hydrocarbon seep using a deep-sea camera system. J. Atmos. Ocean. Technol. 37 (9), 1737–1751. http://dx.doi.org/10.1175/JTECH-D-19-0137.1.
- Römer, M., Hsu, C.-W., Loher, M., MacDonald, I.R., dos Santos Ferreira, C., Pape, T., Mau, S., Bohrmann, G., Sahling, H., 2019. Amount and fate of gas and oil discharged at 3400 m water depth from a natural seep site in the southern gulf of Mexico. Front. Mar. Sci. 6, http://dx.doi.org/10.3389/fmars.2019.00700.
- Romer, M., Sahling, H., Pape, T., Bohrmann, G., Spiess, V., 2012. Quantification of gas bubble emissions from submarine hydrocarbon seeps at the makran continental margin (offshore Pakistan). J. Geophys. Res.-Oceans 117.
- Ruth, D.J., Vernet, M., Perrard, S., Deike, L., 2021. The effect of nonlinear drag on the rise velocity of bubbles in turbulence. J. Fluid Mech. 924, A2. http: //dx.doi.org/10.1017/jfm.2021.556.
- Ruzicka, M.C., 2000. On bubbles rising in line. Int. J. Multiph. Flow. 26, 1141-1181.
- Saffman, P.G., 1956. On the rise of small air bubbles in water. J. Fluid Mech. 1 (3), 249–275. http://dx.doi.org/10.1017/S0022112056000159.
- Salibindla, A.K.R., Masuk, A.U.M., Tan, S., Ni, R., 2020. Lift and drag coefficients of deformable bubbles in intense turbulence determined from bubble rise velocity. J. Fluid Mech. 894, A20. http://dx.doi.org/10.1017/jfm.2020.244.
- Sanada, T., Watanabe, M., Fukano, T., Kariyasaki, A., 2005. Behavior of a single coherent gas bubble chain and surrounding liquid jet flow structure. Chem. Eng. Sci. (ISSN: 0009-2509) 60 (17), 4886–4900. http://dx.doi.org/10.1016/j.ces.2005. 04.010
- Schlichting, H., 1979. Boundary-Layer Theory. McGRAW-HILL, pp. 731-734.
- Shy, S., Tang, C., Fann, S., 1997. A nearly isotropic turbulence generated by a pair of vibrating grids. Exp. Therm Fluid Sci. (ISSN: 0894-1777) 14 (3), 251–262. http://dx.doi.org/10.1016/S0894-1777(96)00111-2.
- Tomiyama, A., Celata, G.P., Hosokawa, S., Yoshida, S., 2002. Terminal velocity of single bubbles in surface tension force dominant regime. Int. J. Multiph. Flow. 28, 1497–1519.
- Tomiyama, A., Kataoka, I., Zun, I., Sakaguchi, T., 1998. Drag coefficients of single bubbles under normal and micro gravity conditions. JSME Int. J. Ser. B 41, 473–479.
- Wang, B., Jun, I., Socolofsky, S.A., DiMarco, S.F., Kessler, J.D., 2020. Dynamics of gas bubbles from a submarine hydrocarbon seep within the hydrate stability zone. Geophys. Res. Lett. 47 (18), e2020GL089256. http://dx.doi.org/10.1029/ 2020GL089256.
- Wang, B., Lai, C.C.K., Socolofsky, S.A., 2019. Mean velocity, spreading and entrainment characteristics of weak bubble plumes in unstratified and stationary water. J. Fluid Mech. 874, 102–130. http://dx.doi.org/10.1017/jfm.2019.461.
- Wang, B., Liao, Q., 2016. Field observations of turbulent dissipation rate profiles immediately below the air-water interface. J. Geophys. Res.: Oceans 121 (6), 4377–4391. http://dx.doi.org/10.1002/2015JC011512.
- Wang, B., Socolofsky, S.A., 2015a. A deep-sea, high-speed, stereoscopic imaging system for in situ measurement of natural seep bubble and droplet characteristics. Deep Sea Res. I 104, 134–148. http://dx.doi.org/10.1016/j.dsr.2015.08.001.
- Wang, B., Socolofsky, S.A., 2015b. On the bubble rise velocity of a continually released bubble chain in still water and with crossflow. Phys. Fluids 27 (10), 103301. http://dx.doi.org/10.1063/1.4932176.
- Wang, B., Socolofsky, S.A., 2019. Characteristics of mean flow and turbulence in bubble-in-chain induced flows. Phys. Rev. Fluids 4, 054302. http://dx.doi.org/10.1103/PhysRevFluids.4.054302.
- Wang, B., Socolofsky, S.A., Breier, J.A., Seewald, J.S., 2016. Observation of bubbles in natural seep flares at MC 118 and GC 600 using in situ quantitative imaging. J. Geophys. Res.: Ocean 121, 2203–2230. http://dx.doi.org/10.1002/2015JC011452.
- Wijngaarden, L.v., 1993. The mean rise velocity of pairwise-interacting bubbles in liquid. J. Fluid Mech. 251, 55–78. http://dx.doi.org/10.1017/S0022112093003337.
- Wu, M., Gharib, M., 2002. Experimental studies on the shape and path of small air bubbles rising in clean water. Phys. Fluids 14 (7), L49–L52. http://dx.doi.org/10. 1063/1.1485767.
- Yang, C.-F., Chi, W.-C., H., v., 2021. Deep-sea turbulence evolution observed by multiple closely spaced instruments. Sci. Rep. 11, 3919. http://dx.doi.org/10.1038/s41598-020-68807-4.

- Yuan, H., Prosperetti, A., 1994. On the in-line motion of two spherical bubbles in a viscous fluid. J. Fluid Mech. 278, 325–349. http://dx.doi.org/10.1017/ S0022112094003733.
- Zhang, J., Ni, M.-J., 2021. A numerical study of a bubble pair rising side by side in external magnetic fields. J. Fluid Mech. 926, A22. http://dx.doi.org/10.1017/jfm. 2021.695.
- Zheng, L., Yapa, P.D., 2000. Buoyant velocity of spherical and nonspherical bubbles/droplets. J. Hydraul. Eng. 126 (11), 852–854. http://dx.doi.org/10.1061/(ASCE)0733-9429(2000)126:11(852).
- Zulberti, A.P., Jones, N.L., Rayson, M.D., Ivey, G.N., 2022. Mean and turbulent characteristics of a bottom mixing-layer forced by a strong surface tide and large amplitude internal waves. J. Geophys. Res.: Oceans 127 (1), e2020JC017055. http://dx.doi.org/10.1029/2020JC017055.